High-Precision Measurement of $\mu_p G_E^p/G_M^p$ at $Q^2 = 3.7$ GeV^2 via Polarization Transfer

A. J. R. Puckett (co-spokesperson and contact person) and K. Joo
*University of Connecticut, Storrs, CT, 06269, USA**

J. Bernauer (co-spokesperson)
Center for Frontiers in Nuclear Science, Department of Physics and Astronomy, Stony Brook University, Stony Brook, NY 11794-3800, USA

A. Schmidt (co-spokesperson) and W. J. Briscoe
George Washington University, Washington, DC 20052, USA

S. Covrig Dusa, M. McCaughan, and B. Wojtsekhowski
Thomas Jefferson National Accelerator Facility, Newport News, VA, 23606, USA

D. Androic
University of Zagreb, Faculty of Science, Croatia

R. Singh
Center for Nuclear Theory, Department of Physics and Astronomy, Stony Brook University, Stony Brook, New York, 11794-3800, USA

S. Širca
Faculty of Mathematics and Physics, U of Ljubljana, Slovenia

P. Markowitz
Florida International University, Miami FL 33199

J. Arrington
Lawrence Berkeley National Laboratory, Berkeley, CA, USA

T. Kolar, J. Lichtenstadt, and E. Piasetzky
Tel Aviv University, Tel Aviv, Israel

M. Nycz
University of Virginia, Charlottesville, VA, 22904, USA

(Dated: May 1, 2024)

I. EXECUTIVE SUMMARY

We request PAC approval for two additional days of beam time for the upcoming "high impact" SBS GEP experiment, to precisely measure the polarization transfer ratio R_p (which equals $\mu_p G_E^p/G_M^p$ in the one-photon approximation) at a squared four-momentum transfer Q^2 of 3.7 GeV^2. These two days of additional beam time would allow us to reach a 1% absolute statistical uncertainty on the ratio R_p at this Q^2, where it would improve the precision over existing polarization data by a factor of four, in the region where the discrepancy between L/T separations and polarization measurements is largest and most significant. The primary motivation for this request is to improve the precision of the polarization data at this Q^2 in anticipation of the comparison to a future measurement using positrons, described in a previous LOI to PAC51 (LOI12-23-008). The PAC51 report on LOI12-23-008 notes:

"The proposed measurement would be a valuable addition to the quantitative study of TPE effects in elastic scattering. A full proposal should include a detailed study of anticipated systematic and statistical uncertainties, along with theory predictions for the expected difference between the polarization transfer observable for positron and electron beams. The latter will be needed in order to assess the physics impact of the measurement."

* puckett@jlab.org

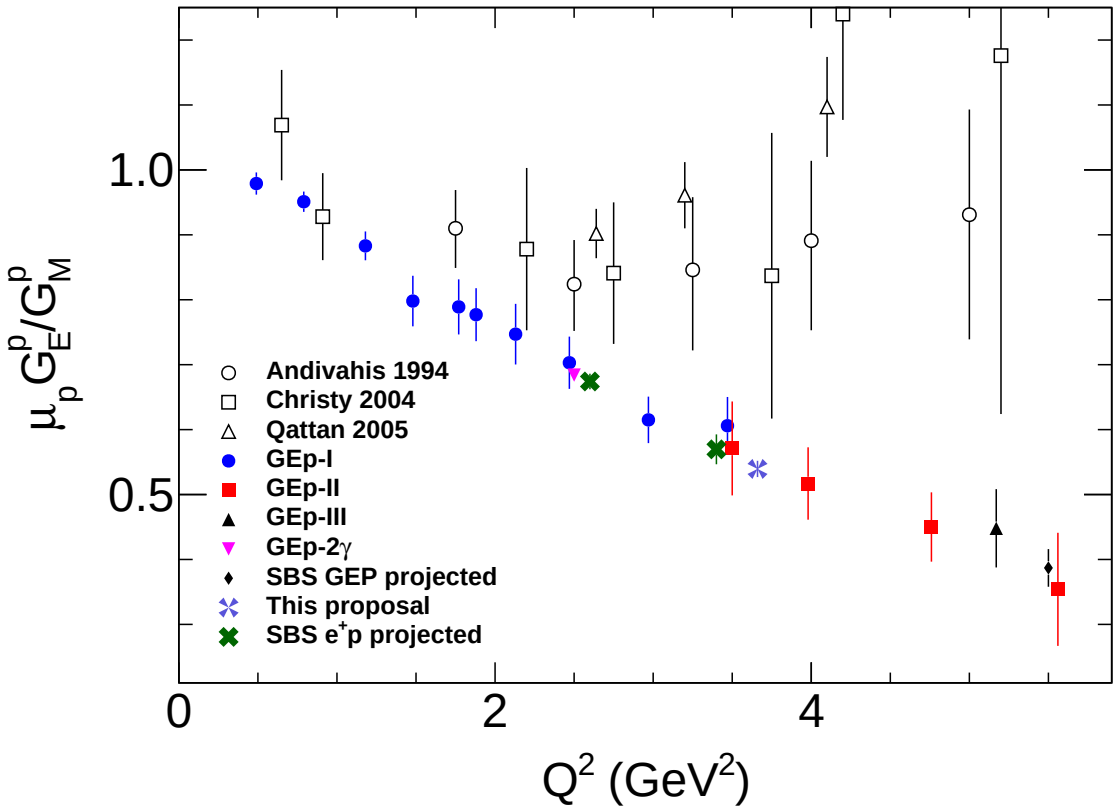

FIG. 1. The proposed measurement in context, compared to planned positron measurements discussed in LOI12-23-008 and in Ref. [1]. Figure adapted from Fig. 3 of Ref. [1].

As noted in the LOI, the precision of the *electron*-proton polarization transfer data in this Q^2 range needs to be improved to facilitate a comparison to *positron* scattering of sufficient precision to discriminate among available TPE calculations. We propose this short measurement *now* because the current experiment schedule provides a one-time opportunity to acquire such data at low cost as a small add-on to an existing experiment, with no required equipment modifications. We postpone a full proposal for the positron measurements to a future PAC, when we expect to have better clarity on the parameters of a polarized positron beam as well as lessons learned and experience gained from the SBS polarization transfer program, toward an optimized experiment design for positron beams. Figure 1 shows the proposed measurement compared to existing cross section and polarization data in this Q^2 region and the future positron measurements envisioned by LOI12-23-008, as first described in Ref. [1].

II. INTRODUCTION

The long-standing discrepancy at large values of four-momentum transfer Q^2 between extractions of the proton form factor ratio G_E^p/G_M^p based on cross section and polarization observables is one of the main scientific motivations for efforts to accelerate high-intensity polarized and unpolarized positron beams in CEBAF [2]. Since the discovery of the rapid decrease of the proton form factor ratio $\mu_p G_E^p/G_M^p$ for $Q^2 \gtrsim 1$ GeV^2 using polarization observables [3–9], enormous efforts in theory and experiment have been ongoing to understand and resolve this discrepancy. On the theoretical side, most investigations have focused on the contribution of hard two-photon-exchange (TPE), which is $\mathcal{O}(\alpha)$ relative to the leading One-Photon-Exchange (OPE) or "Born" term, cannot presently be calculated model-independently, and is neglected in the standard radiative correction procedures to elastic $ep \to ep$ cross section measurements (see Ref. [10] for a recent review of the subject). On the experimental side, three major collaborations (OLYMPUS [11, 12], VEPP-3 [13], and CLAS [14, 15]) have performed precision measurements of e^+p/e^-p elastic scattering cross section ratios in the last decade, in an attempt to directly constrain the size of TPE contributions to unpolarized cross section measurements. Each of these experiments used complementary approaches with different

systematics; however, none reached high enough Q^2 and/or low-enough ϵ with sufficient precision and accuracy to conclusively resolve the discrepancy.

The overarching goals of experimental investigations of hard TPE using positron scattering are to:

1. Determine whether the Rosenbluth/polarization discrepancy in the extraction of $\mu_p G_E^p/G_M^p$ can be fully and self-consistently explained by "hard" TPE (and higher-order QED corrections), as must be the case within a Standard Model paradigm.

2. *Assuming* this is shown to be the case in the Q^2 regime where the discrepancy is most significant, to validate and constrain theoretical calculations of these corrections, elevating hard TPE to the status of a "standard", trusted radiative correction to elastic *ep* scattering observables.

A large part of the CEBAF positron program will consist of precisely mapping the e^+p unpolarized elastic scattering cross sections with a wide coverage in ϵ in the Q^2 range of 1.5-6 GeV^2, where the existing discrepancy is most significant. Despite the Herculean efforts of the previous *positron*-proton scattering experiments to search for and precisely measure *direct* experimental signatures of TPE, the discrepancy seen in *electron*-proton scattering remains by far the most statistically significant direct or indirect evidence for the importance of these effects in charged lepton-proton elastic scattering.

Since the discrepancy first appeared in the polarization observables, an essential ingredient in its eventual conclusive resolution is to investigate whether any discrepancy *also* exists in *either* the comparison of polarization transfer between e^+p and e^-p scattering *and/or* the comparison between Rosenbluth separations and polarization observables in e^+p scattering, independently of the well-established discrepancy for e^-p scattering. No such data currently exist, and such a measurement would provide valuable independent constraints on the "generalized" form factors and their theoretical modeling. We envision a future experimental campaign to measure e^+p polarization transfer to complement e^-p measurements, search for direct evidence of hard TPE, and constrain theoretical models. The first step, after identifying feasible kinematics, is to ensure that there are suitable electron scattering data. We identify a particular kinematic point, which a positron beam would be well-suited to measure, but for which there is no previous electron measurement. The main arguments for the choice of kinematics and precision goals for a future positron measurement were already laid out in our Letter-Of-Intent (LOI12+23-008) to PAC51 as well as our peer-reviewed contribution [1] to the recent topical issue of the European Physical Journal A on the CEBAF positron program [2].

III. THEORETICAL FORMALISM

In the OPE approximation, the polarization transferred to the scattered proton in the elastic scattering of longitudinally polarized electrons/positrons by unpolarized protons has longitudinal (P_ℓ) and transverse (P_t) components with respect to the momentum transfer parallel to the lepton scattering plane, given by:

$$P_t = -\sqrt{\frac{2\epsilon(1-\epsilon)}{\tau}}\frac{r}{1+\frac{\epsilon}{\tau}r^2} \tag{1}$$

$$P_\ell = \frac{\sqrt{1-\epsilon^2}}{1+\frac{\epsilon}{\tau}r^2}, \tag{2}$$

where $r \equiv G_E^p/G_M^p$ is the ratio of the Sachs electric and magnetic form factors, $\tau \equiv \frac{Q^2}{4M^2}$ with M the proton mass, and $\epsilon \equiv \left[1+2(1+\tau)\tan^2\left(\frac{\theta_e}{2}\right)\right]^{-1}$, with θ_e the lab-frame scattering angle of the electron, is the longitudinal polarization of the virtual photon (in OPE). The ratio of the two polarization transfer components is directly proportional to the form factor ratio by a precisely measurable kinematic factor:

$$\mu_p\frac{G_E^p}{G_M^p} = -\mu_p\frac{P_t}{P_\ell}\sqrt{\frac{\tau(1+\epsilon)}{2\epsilon}} = -\mu_p\frac{P_t}{P_\ell}\frac{E_e+E_e'}{2M}\tan\left(\frac{\theta_e}{2}\right), \tag{3}$$

where the last expression in Eq. 3 holds in the proton rest (lab) frame, with E_e (E_e') the incident (scattered) electron energy, and μ_p the proton's magnetic moment in nuclear magnetons.

The simultaneous measurement of both recoil polarization components and the rapid beam helicity reversal lead to cancellation of most major sources of experimental systematic uncertainty. While polarization transfer is less sensitive to the effects of radiative corrections and hard TPE, it is not immune. Following the formalism of Ref. [16], one finds

that

$$\frac{P_t}{P_\ell} = -\sqrt{\frac{2\epsilon}{\tau(1+\epsilon)}}\frac{G_E}{G_M} \times \left[1 \pm \mathrm{Re}\left(\frac{\delta\widetilde{G}_M}{G_M}\right) \pm \frac{1}{G_E}\mathrm{Re}\left(\delta\widetilde{G}_E + \frac{\nu}{M^2}\widetilde{F}_3\right) \mp \frac{2}{G_M}\mathrm{Re}\left(\delta\widetilde{G}_M + \frac{\epsilon\nu}{(1+\epsilon)M^2}\widetilde{F}_3\right) + \mathcal{O}(\alpha^2)\right], \tag{4}$$

with $\nu \equiv (p_e + p_{e'})_\mu (p_p + p_{p'})^\mu$, and where $\delta\widetilde{G}_E$, $\delta\widetilde{G}_M$, and $\widetilde{F}_3$ are additional form factors that become non-zero when moving beyond the one-photon exchange approximation and, crucially, depend on both Q^2 and ϵ, whereas the one-photon-exchange form factors depend only on Q^2. The correction terms $\delta\widetilde{G}_E$, $\delta\widetilde{G}_M$, and $\widetilde{F}_3$ are $\mathcal{O}(\alpha)$ relative to the one-photon-exchange form factors G_E, G_M. The $\pm/\mp$ symbols in Eq. (4) indicate the sign with which the two-photon-exchange amplitudes enter the observable P_t/P_ℓ depending on the lepton charge, with the upper (lower) symbol indicating the appropriate sign for $e^-(e^+)$ beams. This particular dependence on new form factors is slightly different than what one finds when taking a positron to electron cross section ratio:

$$\frac{\sigma_{e^+p}}{\sigma_{e^-p}} = 1 + 4G_M\mathrm{Re}\left(\delta\widetilde{G}_M + \frac{\epsilon\nu}{M^2}\widetilde{F}_3\right) - \frac{4\epsilon}{\tau}G_E\mathrm{Re}\left(\delta\widetilde{G}_E + \frac{\nu}{M^2}\widetilde{F}_3\right) + \mathcal{O}(\alpha^2). \tag{5}$$

A measurement of the difference in polarization transfer between electron and positron scattering therefore adds information about TPE in addition to what can be learned from cross section ratios alone. Moreover, as described in a separate proposal to PAC51, precise Rosenbluth separations of e^+p scattering will be pursued using the precision spectrometers in Hall C, in the same Q^2 range as the proposed polarization transfer measurements using SBS. These Rosenbluth separations of e^+p scattering can then be directly compared to the e^+p polarization transfer measurements described in LOI12-23-008. Such comparisons will be extremely interesting in addition to the comparison with existing and planned e^-p polarization transfer data, given that the existing discrepancy between cross sections and polarization observables in e^-p scattering is *much* greater than the combined uncertainty of the two observables. If a discrepancy of similar magnitude exists for e^+p scattering, as might reasonably be expected if hard TPE is the physical mechanism for the discrepancy seen in e^-p scattering, it will easily be seen, even in an experiment only half as precise as the stated goal of LOI12-23-008.

IV. BACKGROUND ON TWO-PHOTON EXCHANGE

A. Theoretical Approaches

The leading hypothesis for the cause of the proton form factor discrepancy is a radiative effect called hard two-photon exchange, which is neglected in standard radiative correction formulae, and may bias the Rosenbluth separation and polarization transfer techniques differently [17, 18]. Standard radiative correction procedures, such as those of Mo and Tsai [19], or Maximon and Tjon [20], treat two-photon exchange (TPE) in the so-called "soft-limit," an approximation in which one of the photons carries negligible four-momentum. This approximation makes the TPE diagram tractable without model-dependence. The TPE contribution beyond the soft-limit is referred to as "hard two-photon exchange," or hard TPE. It should be noted that two-photon exchange has to be treated in order to cancel divergences in bremsstrahlung terms. The set of diagrams treated by standard radiative corrections procedures are shown in Fig. 2.

One of the challenges preventing incorporation of hard TPE into standard radiative corrections prescriptions is difficulty in calculating the TPE diagram without adding significant model dependence. The TPE diagram has an off-shell hadronic propagator, which requires some QCD input in order to be evaluated. In general, there are two classes of approaches: hadronic methods and partonic methods, which are described in the following sections. There are also a handful of alternative theoretical approaches which fit in neither category, some of which suggest that TPE cannot be the cause of the form factor discrepancy (e.g. [21]).

Efforts to advance our understanding of TPE and of radiative corrections more generally is an active area of research, with applications beyond merely the discrepancy in the proton form factors. TPE is a significant correction in scattering experiments at low Q^2 to determine the proton radius. The TPE diagram shares many of the same challenges with the γZ box diagram that is a major radiative correction in parity-violating electron scattering, and

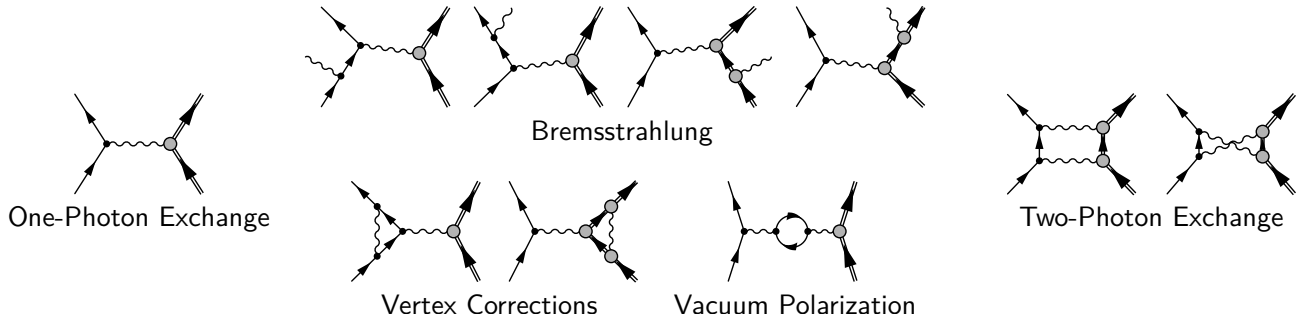

FIG. 2. Diagrams treated in standard radiative corrections to elastic electron scattering

with the γW box diagram in nuclear β-decay. An Ad-Hoc Workshop on Radiative Corrections, held (remotely) in 2020 by CFNS at Stony Brook produced a white paper [22] on current challenges in radiative corrections. This was followed by a workshop at the ECT in Trento in 2022 with a second paper forthcoming [23].

Hadronic Methods

In hadronic methods, the off-shell propagator is expanded as a sum of on-shell intermediate hadronic states. This series is, in principle, infinite, containing all baryons with quantum numbers accessible from photon-nucleon coupling. In practice, the higher mass resonances contribute less and less with mass, and the expansion can be truncated to get an approximate result. Additional model dependence comes from the assumptions about the transition form factors for each intermediate state. Early works used the direct evaluation of loop integrals [18, 24], but the flexibility of hadronic calculations have greatly improved by using dispersive methods [25–29]. The most advanced dispersive hadronic calculation incorporates contributions from the nucleon as well as all $N*$ and Δ resonances with masses up to 1.8 GeV [29].

Hadronic approaches should perform better at low momentum transfer, and calculations are typically not performed above $Q^2 > 3$ GeV$^2/c^2$. In that limit, however, the results of hadronic calculations suggest that hard TPE would drive the apparent $\mu_p G_E/G_M$ extracted from unpolarized cross sections up and away from the results of polarization transfer [18, 30]. Nevertheless, hadronic calculations do show some variance based on different model assumptions used and which intermediate states are included.

Partonic Methods

Partonic methods model the hard interaction of the two exchanged photons with individual quarks, but then embed those quarks inside the proton using a model of the proton's partonic structure—either its distribution amplitudes (DAs) or generalized parton distributions (GPDs). This approach is more accurate at high momentum transfers where the factorization between the hard scattering and the soft structure are on firmer ground, ideally above $Q^2 > 5$ GeV$^2/c^2$. The accuracy is only as good, however, as our understanding of the proton's multi-dimensional structure. Examples of partonic estimates include Refs. [31–35].

Phenomenology

There is a class of phenomenological two-photon exchange estimates that use experimental data to estimate the magnitude of the two-photon exchange amplitude, making the assumption that hard TPE is the sole cause of the proton form factor discrepancy [36–40]. This amounts to determining how much of a hard TPE effect would be necessary to fully resolve the discrepancy. If the measured TPE differed substantially from these phenomenological predictions, this would be evidence that factors other than hard TPE are responsible for the discrepancy. However, even modestly different assumptions lead to a wide range of phenomenological estimates, which implies that even the magnitude of the discrepancy is not well-constrained.

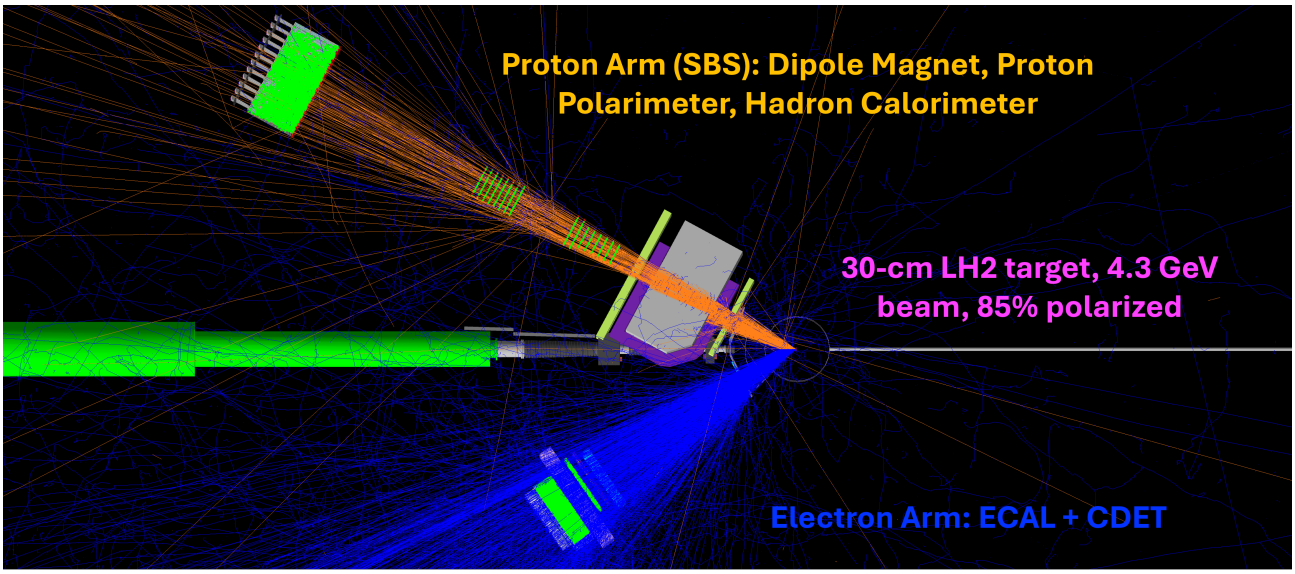

FIG. 3. Layout of the proposed experiment in the GEANT4-based Monte Carlo simulation of the SBS GEP setup (top view), showing 500 elastic $ep \to ep$ events tracked through the detectors, indicating the rough acceptance matching between electron and proton arms. The blue and orange lines represent electron and proton trajectories, respectively, while the green dots represent "hits" in sensitive volumes (GEMs, ECAL lead glass, HCAL and CDET scintillators). The incident beam direction is from right to left in this figure (in case it wasn't obvious).

V. EXPERIMENT DETAILS

A. The SBS GEP experiment and apparatus

Experiment E12-07-109 [41, 42], first approved by JLab PAC32 in 2007, aims to measure the proton form factor ratio $\mu_p G_E^p/G_M^p$ to $Q^2 = 12$ GeV^2 with high precision. The experiment was the original motivation for the construction of the Super BigBite Spectrometer. The experiment was given a "high impact" designation by JLab's PAC41, was re-approved at its Jeopardy evaluation in 2019 [42], and passed JLab's experiment readiness review (ERR) process in 2023. It is now on the published experiment schedule and expected to start in the fall of 2024.

The upcoming SBS GEP run presents a unique, one-time opportunity to obtain a high-precision measurement of polarization transfer in electron-proton elastic scattering at a moderately large Q^2 of about 3.66 GeV^2 with a goal of 1% absolute statistical uncertainty on the ratio $\mu_p G_E^p/G_M^p$, anticipating the comparison to a future positron measurement. Given the large acceptance and high luminosity capability of SBS, such a measurement will only require 2 days of additional beam time for the SBS GEP run, plus the approximately two days of overhead associated with a pass change and spectrometer movement. The proposed short addition to the SBS GEP run will improve the precision of the proton FF ratio by a factor of several at this Q^2, and will greatly aid the commissioning of the apparatus and systematics control for the higher Q^2 measurements requiring most of the approved beam time. In this section we give a brief overview of the experimental apparatus. For additional technical details, the reader is referred to the original [41] and jeopardy [42] proposals, as well as the ERR documentation. In this proposal, we do not address in detail all the technical challenges associated with trigger efficiencies and DAQ rates, detector background rates/occupancies, and thermal annealing, as these aspects were already exhaustively reviewed by two previous PACs, the annual DOE reviews during the construction of the formal SBS project, and the JLab ERR committee. Suffice it to say that all of these challenges become less difficult at lower Q^2, and this measurement, if approved, would be by far the easiest of the four. The only question raised by this proposal to this PAC is whether to approve a small amount of extra beam time for an opportunistic, high-precision measurement that is needed by a future positron polarization transfer program, which PAC51 judged would be "a valuable addition to the quantitative study of TPE in elastic scattering" in its evaluation of LOI12-23-008.

Figure 3 shows the layout of the proposed add-on measurement to the upcoming SBS GEP run. The SBS sits at a central angle of 28.5 degrees on beam right, while the electron arm sits at a central angle of 35 degrees on beam left. Electrons of energy 4.3 GeV (standard 2nd-pass CEBAF energy anticipated during SBS GEP run) with 85% longitudinal polarization will be scattered from the 30-cm liquid hydrogen target that is being prepared for GEP.

The proton arm consists of the SBS dipole magnet, GEM-based trackers for kinematic reconstruction and proton polarimetry, a 56 cm-thick CH_2 (HDPE) analyzer to measure the polarization of elastically scattered protons, and a hadron calorimeter (HCAL) to provide an efficient and selective trigger for the events of interest for polarimetry. The electron arm consists of the high-temperature lead-glass Electron Calorimeter (ECAL) and the scintillator-based Coordinate Detector (CDET).

1. Super BigBite Spectrometer

Starting from the target, each component of the SBS proton arm performs several important functions. The dipole magnet, which can reach a maximum $\int B_\perp dl \approx 2.4$ T·m when equipped with "pole shims" to increase the field strength in the magnet gap, is used for momentum analysis of scattered protons and to precess the longitudinal component of the proton's polarization into a transverse component that can be measured by the secondary scattering in the CH_2 analyzer. The magnet also shields the detectors from low-energy charged particles.

Eight layers of Gas Electron Multipliers (GEMs) in the Front Tracker (FT), built by the University of Virginia, are used to track elastically scattered protons and precisely reconstruct the reaction kinematics and the interaction vertex. The front tracking results are also used to define the incident trajectory for measurement of the angular distribution of the secondary scattering in the CH_2, and for the calculation of proton spin precession in the SBS dipole field. Eight more layers of GEMs after the CH_2 analyzer constitute the back tracker (FPP). These GEMs measure the scattered proton trajectories to reconstruct polar and azimuthal angles of the secondary scattering. Most of the front tracker and back tracker GEMs have already been operating in Hall A in the SBS neutron form factor experiments since Oct. 2021. The SBS Hadron Calorimeter (HCAL) serves three main functions in the GEP experiment. First and most importantly, HCAL provides an efficient and selective trigger for the events of interest for recoil proton polarimetry in coincidence with ECAL. Secondly, the spatial resolution of HCAL provides a helpful constraint to aid tracking in the rear GEMs. Thirdly, the requirement of a large energy deposit in HCAL preferentially selects forward elastic proton-nucleus scattering events with high analyzing power. It is expected that this energy selectivity may increase the effective analyzing power of the polarimeter by up to 30% [43] relative to previous experiments of this type (see, e.g., Ref. [9]). However, this is not assumed in our statistical uncertainty projection or beam time request.

2. Electron Calorimeter and Coordinate Detector

The novel high-temperature lead-glass electromagnetic calorimeter (ECAL) is used to detect elastically scattered electrons in coincidence with the scattered protons, with a large solid-angle acceptance that is kinematically matched to the fixed solid-angle acceptance of the proton arm. It consists of approximately 1,700 lead-glass blocks of dimension $4.2 \times 4.2 \times 34.3$ cm^3 each. The Cherenkov light produced by the electromagnetic cascade is recorded by PMTs coupled to the lead-glass via extended light guides. The lead-glass is embedded in a $\approx$ 225 °C oven for continuous thermal annealing of radiation damage to maintain stable transparency and energy resolution in the high-radiation environment of Hall A. ECAL is augmented by a highly-segmented, scintillator-based "Coordinate Detector" (CDET), that will act as a veto for high-energy photons from π_0 decay that are not otherwise distinguishable from electrons of similar energy, and will measure the vertical coordinates of the electron with a resolution 2-3 times better than the spatial resolution of the calorimeter.

The electron arm serves several important functions. First and most importantly, the good energy resolution of lead-glass (with continuous thermal annealing) provides for a highly efficient and selective trigger at an energy threshold of approximately 80-85% of the elastically scattered electron energy. To achieve a manageable trigger rate for the DAQ system of 2-3 kHz at the planned luminosity, the two-body angular correlation between ECAL and HCAL is implemented at the trigger level, allowing roughly 3-5 times greater background rejection as compared to a naive coincidence of inclusive single-arm ECAL and HCAL triggers. The second and equally important function of ECAL is to define the region-of-interest for track-finding in the SBS front tracker, again exploiting the two-body angular correlation between electron and proton. The front tracker reconstruction would not be possible at the proposed luminosities without the very stringent constraints imposed by the reconstructed electron scattering angles and the two-body kinematics of the reaction of interest. The third (and also very important) function of the electron arm is to reject inelastic backgrounds in the offline analysis.

B. Monte Carlo Simulation: Kinematics, Event Rates, and Polarimetry Figure-of-Merit

The choice of spectrometer angles for this proposal is driven by the physics goal and by the constraints of the actual experiment design. The maximum central angle of the SBS consistent with the acceptance of the GEP scattering chamber is 28.5 degrees. This essentially dictates the range of Q^2 that will be accepted by the proton arm at 2nd pass. The polar angle acceptance of SBS is approximately ± 3 degrees relative to the central angle. The central Q^2 value corresponding to an SBS central angle of 28.5 degrees with a beam energy of 4.3 GeV is 3.8 GeV^2. The implied central angle for the electron is 36.5 degrees. Given the large solid angle acceptance of ECAL, it is not critical to place ECAL at exactly the central angle dictated by SBS. As can be seen qualitatively in Fig. 3, the solid angle matching between ECAL and SBS at a central angle of 35 degrees at a distance of 5 meters from the target is quite good, and the coverage gained by placing ECAL at a larger central angle would be outside the useful acceptance of the GEP scattering chamber in any case.

To estimate the event rates and beam time requirements for this proposal, elastic $ep \to ep$ scattering events were generated and tracked through the GEANT4 simulation of the experiment with realistic magnetic field map and detector response. The angle generation limits were chosen wide enough to populate the full acceptance of SBS for elastically scattered protons. The following assumptions were made:

- Beam energy 4.3 GeV
- Beam longitudinal polarization 85%
- Beam current 50 μA
- Liquid hydrogen target, 30 cm thickness
- SBS at 28.5 degrees
- ECAL at 35 degrees and 5 meters from the target.
- SBS magnetic field at 39% of maximum (optimizes acceptance)
- $\mathbf{p}$+CH_2 analyzing power parametrized according to the results described in Ref. [9] (worst-case assumption).
- *ep* elastic cross section given by Rosenbluth formula in one-photon-exchange approximation, with the "GMp12" parametrization of the "effective" proton form factors [44]
- A simplified approximation of the coincidence trigger logic was achieved in the Monte Carlo by requiring total energy deposits in ECAL (HCAL) of at least 1.4 GeV (70 MeV).

The "figure-of-merit" of the experiment was estimated by selecting all events passing the simplified, approximate "trigger" logic with good proton tracks reconstructed in both front and rear GEM trackers. In addition, the distance of closest approach between front and back tracks was required to be less than 1 cm and the point of closest approach between front and back tracks was required to lie within the physical extent of the analyzer, with some added tolerance for resolution. The "figure-of-merit" for the purpose of this proposal is defined as the following sum over all events satisfying $0.07 \leq p_T \equiv p_p \sin(\theta_{FPP}) \leq 1.0$ GeV:

$$\mathcal{F} \equiv \sum_{i=1}^{N_{event}} (P_e A_y)^2, \tag{6}$$

where P_e is the beam polarization and $A_y \equiv A_y(p_p, p_T)$ is the analyzing power, calculated for each event from the aforementioned parametrization [9] of the Hall C GEp-III analyzing power data for CH_2. The statistical uncertainties of the measured proton polarization components at the focal plane are given by:

$$\Delta P_{x,y}^{FPP} = \sqrt{\frac{2}{\mathcal{F}}} \tag{7}$$

In the "ideal dipole" approximation to the spin precession in SBS, the measured polarization components are related to the transferred polarization components P_t and P_ℓ by:

$$P_y^{FPP} \approx P_t \tag{8}$$

$$P_x^{FPP} \approx -P_\ell \sin(\chi), \tag{9}$$

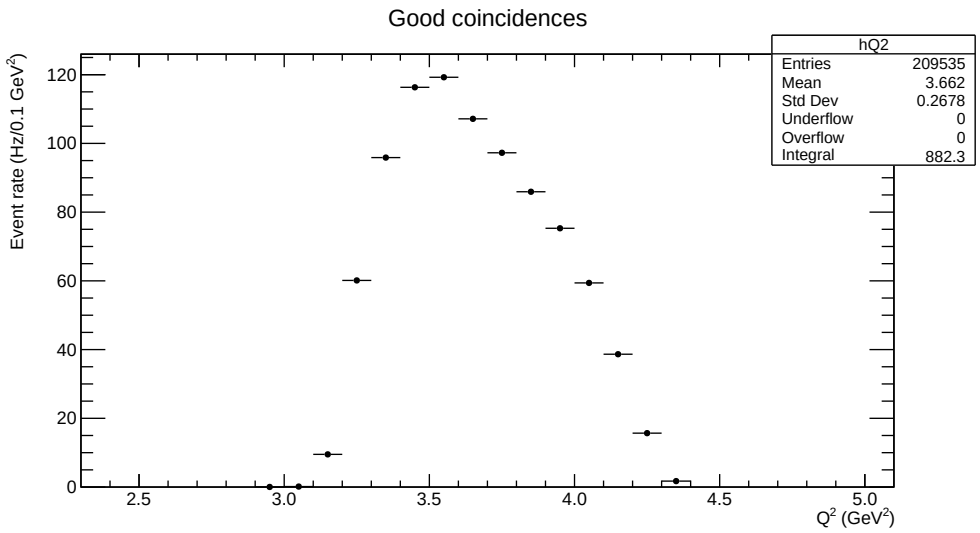

FIG. 4. Rate-weighted Q^2 distribution of events passing the "trigger" cuts (energy threshold on ECAL and HCAL). The total elastic *ep* event rate with these cuts is approximately 900 Hz at a beam current of 50 μA.

where $\chi \equiv \gamma\kappa_p\theta_{bend}$ is the precession angle of the proton spin relative to its trajectory. The proton form factor ratio is then obtained from

$$R_p \equiv \mu_p \frac{G_E^p}{G_M^p} = -\mu_p \frac{P_t}{P_\ell}\sqrt{\frac{\tau(1+\epsilon)}{2\epsilon}}, \tag{10}$$

where the kinematic factor on the right-hand-side of Eq. (10) is calculated as its rate-weighted average value over all simulated events passing the cuts. The statistical uncertainty of the form factor ratio is given by

$$\left(\frac{\Delta R}{R}\right)^2 = \left(\frac{\Delta P_t}{P_t}\right)^2 + \left(\frac{\Delta P_\ell}{P_\ell}\right)^2, \tag{11}$$

neglecting the generally small covariance between P_t and P_ℓ (which would of course be accounted for in a real physics analysis, but is negligible for this purpose).

Figure 4 shows the rate-weighted Q^2 distribution of events passing the "trigger" cuts (threshold on energy deposit in both calorimeters). The total event rate assuming 50 μA beam current on 30-cm liquid hydrogen is about 900 Hz. Figure 5 shows the polar scattering angle distribution in the FPP, and the distribution of the pseudo-transverse momentum $p_T \equiv p_p \sin(\theta_{FPP})$. The polarimeter "efficiency" defined as the fraction of all events with polar scattering angles in the useful range, is approximately 26%.

Figure 6 shows the distance of closest approach s_{close} between incident and scattered proton tracks in the polarimeter. Good events for polarimetry are required to have $s_{close} < 1$ cm. Figure 7 shows the distribution of the point of closest approach between incident and scattered tracks in the polarimeter. A loose cut is placed to select the physical extent of the CH_2 analyzer with some added tolerance for resolution.

Figure 8 shows the reconstructed beam helicity asymmetry as a function of the azimuthal scattering angle. The rapid beam helicity reversal (typically 30 Hz) cancels any instrumental asymmetry associated with detector acceptance/efficiency, and also cancels the effects of slow drifts in other experimental parameters such as luminosity. This results in a pure sinusoidal asymmetry whose amplitude is proportional to the proton's transverse polarization, and whose phase is determined by the ratio of the two transverse components measured by the polarimeter:

$$\text{Asymmetry} = P_e \bar{A}_y \left[P_y^{FPP}\cos(\phi) - P_x^{FPP}\sin(\phi)\right] \tag{12}$$

The simulation used to estimate the polarimeter figure of merit resulted in about 420,000 events passing the trigger cuts, of which roughly 109,000 (or about 26% of the total) passed all the polarimeter event selection cuts. It is these 109,000 events on which the asymmetry extraction shown in Fig. 8 is based. The asymmetry shown in Fig. 8 is equivalent to approximately 8 minutes of beam time in the proposed experiment.

The calculation of proton spin precession has historically been an important source of systematic uncertainty in polarization transfer experiments [5, 8, 9]. The precession in the SBS dipole, however, is much simpler than in

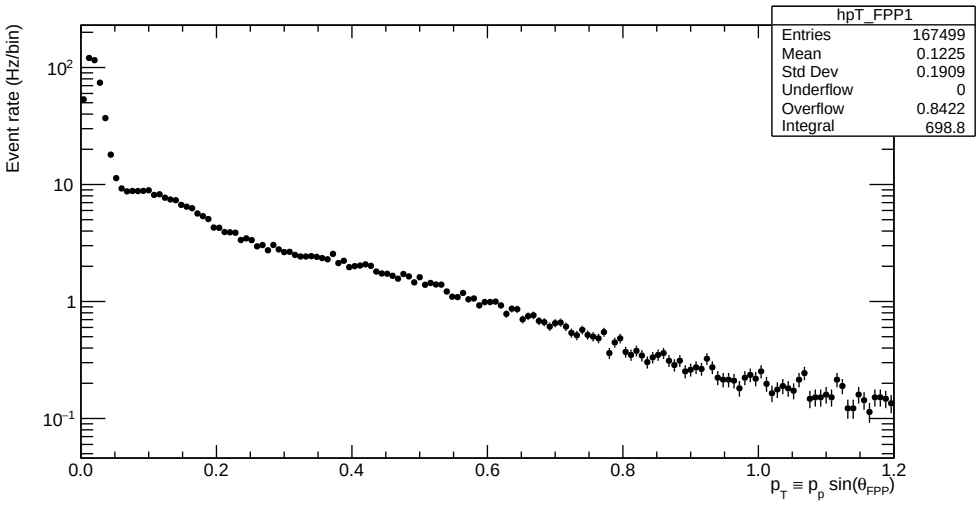

FIG. 5. Polar angle distribution in the SBS FPP (rate-weighted), plotted in terms of the pseudo-transverse momentum $p_T \equiv p_p \sin(\theta_{FPP})$. The useful range of scattering for polarimetry is $0.07 \leq p_T(GeV) \leq 1.0$, or roughly 1.4-21 degrees.

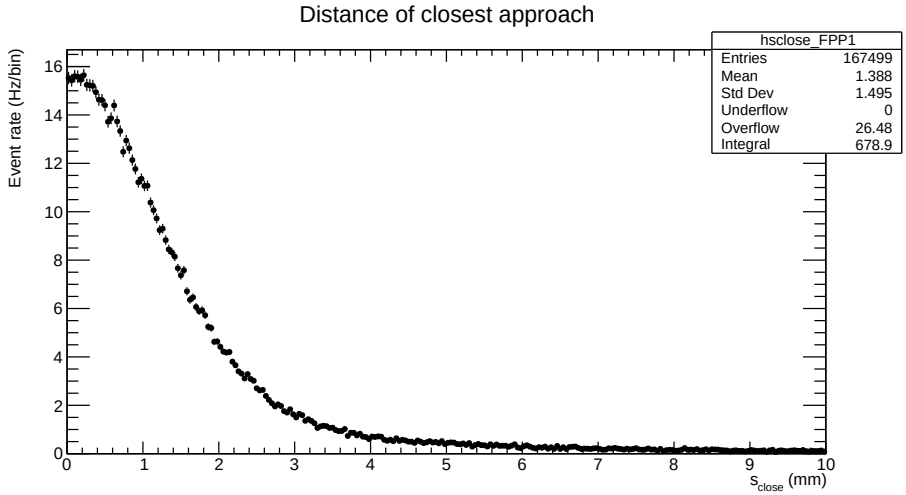

FIG. 6. Distance of closest approach between front and back tracks. A cut $s_{close} < 1$ cm was used to select good events for polarimetry.

previous experiments that used focusing magnetic spectrometers with several quadrupoles in addition to a momentum-analyzing dipole. Figure 9 shows a side view of the SBS field map used in the simulation, scaled to the field strength that optimizes the coincidence *ep* acceptance and therefore the event rate. At 39% of its maximum field strength, the SBS dipole field precesses the proton spin by an average of 33 degrees away from longitudinal (see Figure 10). The precession angle is nearly constant throughout the acceptance. It only has a small negative correlation with the proton momentum within the acceptance. The reason for this simple behavior is the near-perfect cancellation between the relativistic γ factor for the proton, which increases roughly proportionally to the momentum p, and the trajectory bend angle, which is inversely proportional to p, such that the product $\chi = \gamma \kappa_p \theta_{bend}$ is approximately constant within the SBS acceptance, except at lower momenta for which protons are less relativistic and see a greater effective field integral along their more strongly curved trajectories. Figure 10 shows the distribution of χ and the correlation between χ and the proton momentum p_p in the proposed experiment. The full GEANT4 spin tracking machinery using the BMT equation for protons agrees very well with the simple ideal dipole approximation throughout the acceptance. As such, both the precession calculation and the momentum reconstruction can be independently calibrated using

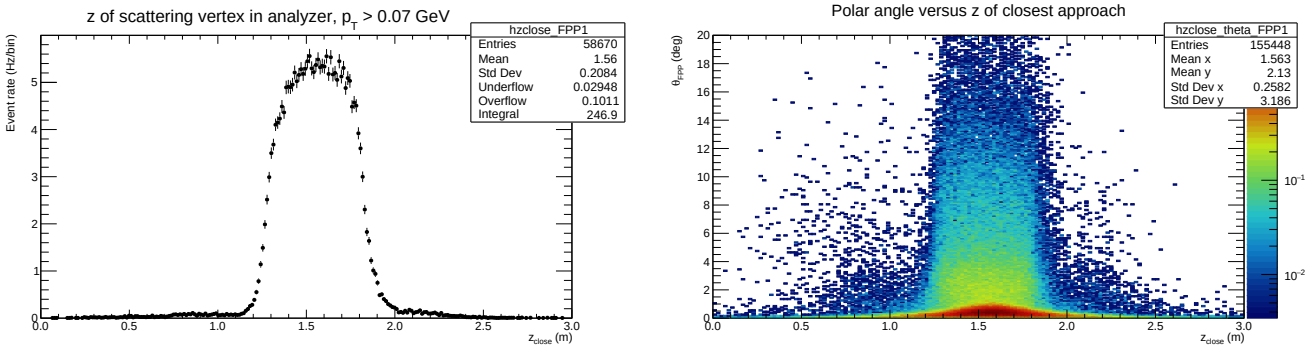

FIG. 7. z of point of closest approach between front and back tracks, for events with $p_T > 0.07$ GeV (top), and versus the polar scattering angle θ_{FPP} (bottom). A cut $1.2 \leq z_{close}(\mathrm{m}) \leq 1.9$, together with minimum p_T cut, is used to select events for polarimetry.

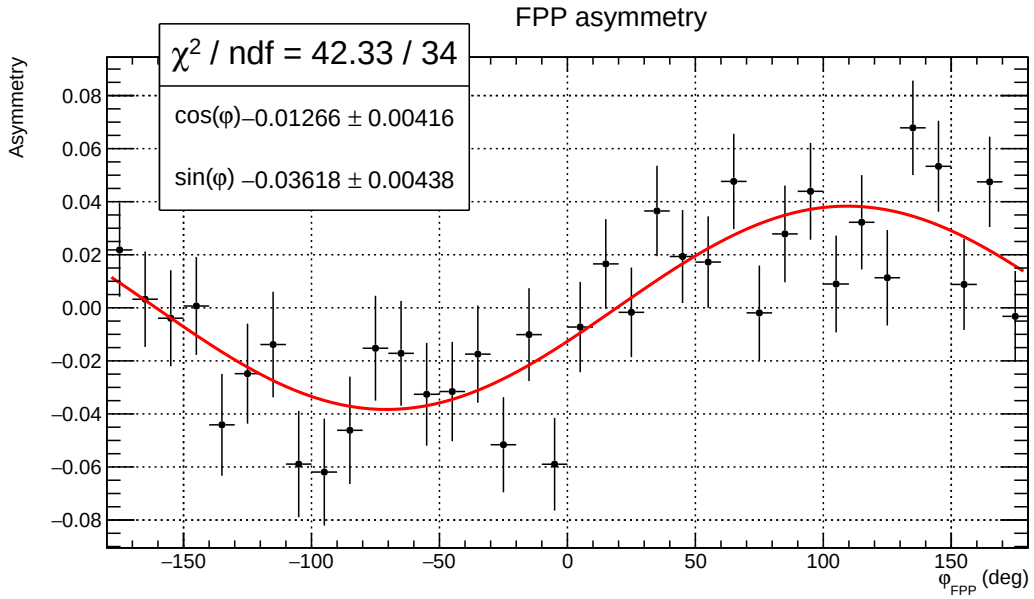

FIG. 8. Beam helicity asymmetry $(N_+(\varphi) - N_-(\varphi))/(N_+(\varphi) + N_-(\varphi))$ for the roughly 109,000 simulated events that passed the coincidence trigger and FPP event selection criteria (approximately 26% of the total). The Monte Carlo statistics shown in this example are equivalent to 8 minutes of beam time in the proposed experiment. The fit function is $A(\varphi) = c_1 \cos(\varphi) - s_1 \sin(\varphi)$, where c_1 and s_1 are the extracted moments shown on the plot. **NOTE TO SELF: Replace with a higher-statistics simulation before the PAC meeting**.

several redundant cross checks to precisely determine the trajectory bend angle for elastically scattered protons of known momentum, without relying on optics models calculated from the field map.

The ideal precession angle for measuring P_ℓ would be 90 degrees (or any odd-integer multiple thereof giving $|\sin(\chi)| = 1$). At its maximum field setting, the SBS dipole will precess the spin of a proton by about 81 degrees, almost independently of momentum. However, the resulting field would bend the trajectory of the 2.8-GeV protons in the proposed measurement by nearly 15 degrees, which would lead to an unacceptable loss of coincidence ep acceptance that would far outweigh any enhanced sensitivity to P_ℓ. Moreover, even for the 33-degree precession angle resulting from the field that optimizes the acceptance, the form factor ratio uncertainty is still dominated by the measurement of P_t. This is clearly evident in Fig. 8, which shows that the $-\sin(\varphi)$ (left-right) asymmetry proportional to $P_\ell \sin\chi$ is still nearly 3 times as big as the $\cos(\varphi)$ (up-down) asymmetry proportional to P_t. The acceptance-averaged value of $\sin(\chi)$ is 0.55, while the average values of the polarization transfer components are $\langle P_t \rangle = -0.115$ and $\langle P_\ell \rangle = 0.686$, respectively. As such, despite the suboptimal precession angle, P_ℓ is still determined with approximately three times

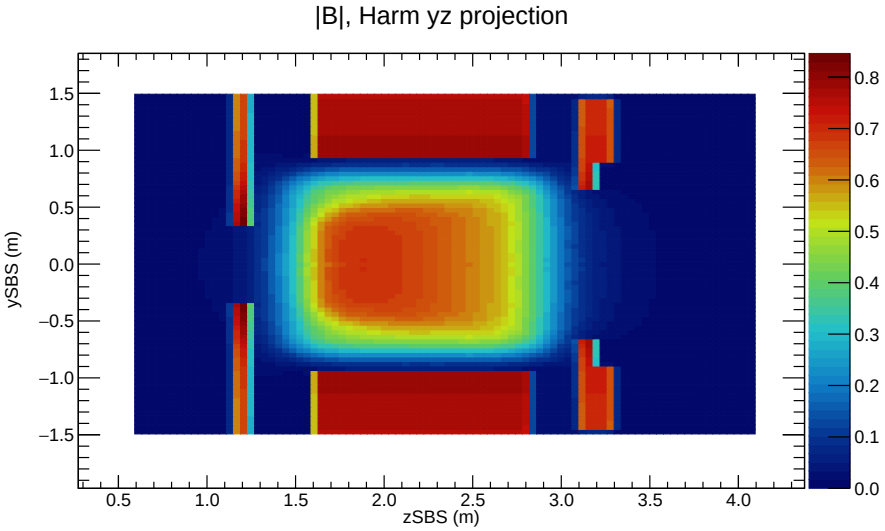

FIG. 9. Magnetic field map in SBS used for the calculation of spin precession and charged-particle transport in the proposed experiment. Figure shows the total field magnitude (in Tesla) in a vertical cross section taken through the midpoint of the magnet, as viewed from the large-angle side. The direction of particle motion is from left to right in this picture.

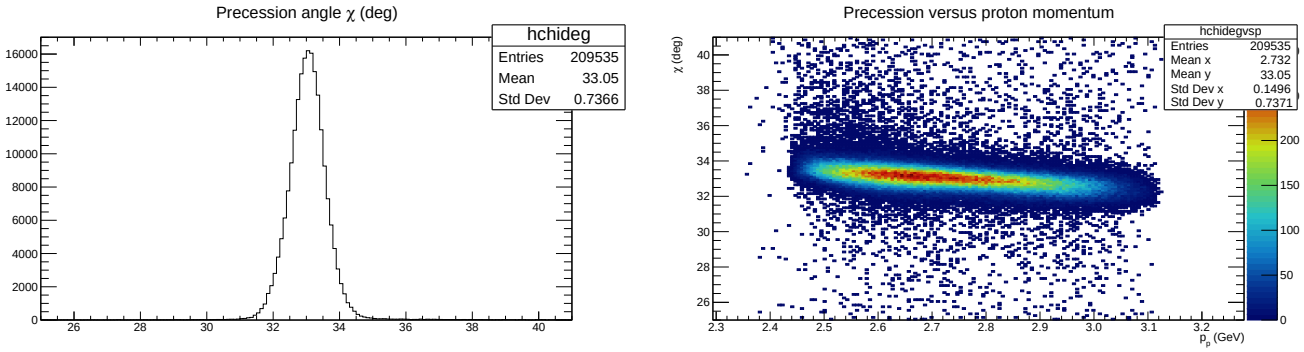

FIG. 10. Left: Distribution of precession angle χ in the proposed measurement. Right: Correlation between precession angle χ and the proton momentum p_p. See text for details.

better relative precision than P_t, which dominates the ratio uncertainty. Table I summarizes the simulation results for the proposed experiment parameters and the assumptions underlying our beam time request.

C. Systematic Uncertainties

The polarization transfer method has few significant sources of systematic uncertainty. This is because the simultaneous measurement of P_t, P_ℓ, and their ratio in a recoil polarimeter determines the form factor ratio directly via equation (10). This eliminates all systematics associated with required kinematics changes that plague the Rosenbluth method in particular. Other relevant quantities for the *statistical* uncertainty, like the beam polarization and the polarimeter analyzing power, contribute essentially nothing to the systematic uncertainty, as they cancel in the ratio P_t/P_ℓ. The rapid beam helicity reversal eliminates false/instrumental asymmetries associated with non-uniformities of the polarimeter acceptance/detection efficiency. The kinematic factor in Eq. (10) is easily measured to an accuracy of 10^{-3} or better on an event-by-event basis. Moreover, the elastic ep reaction is largely "self-calibrating" with respect to most aspects of event reconstruction and polarimetry.

There are still several important sources of systematic error in the result of a polarization transfer measurement. These include the effects of systematic errors in the reconstructed proton kinematics on the event-by-event calculation of the proton's spin precession through the SBS dipole, uncertainties in the precession calculation itself due to

TABLE I. Summary of the Monte Carlo simulation results for the proposed measurement. Quantities enclosed by $\langle \ldots \rangle$ represent rate-weighted, acceptance-averaged values.

Beam energy E_e (GeV)	4.3
Electron scattering angle $\langle \theta_e \rangle$ (deg)	35.12
Proton scattering angle $\langle \theta_p \rangle$ (deg)	29.6
Scattered electron energy $\langle E'_e \rangle$ (GeV)	2.35
Scattered proton momentum $\langle p_p \rangle$ (GeV)	2.73
Squared four-momentum transfer $\langle Q^2 \rangle$ (GeV^2)	3.66
Virtual photon polarization $\langle \epsilon \rangle$	0.71
Spin precession: $\langle \sin(\chi) \rangle$	0.546
Analyzing power $\langle A_y \rangle$ (GEp-III parametrization)	0.114
Event rate at 50 μA (trigger cuts only, Hz)	882
Polarimeter "efficiency"[a]	0.26
Transverse polarization transfer $\langle P_t \rangle$	-0.115
Longitudinal polarization transfer $\langle P_\ell \rangle$	0.686
Kinematic factor (see Eq. (10)) $\left\langle \mu_p \sqrt{\frac{\tau(1+\epsilon)}{2\epsilon}} \right\rangle$	3.13
PAC Days at 50 μA	2
Absolute $\Delta_{stat}\left(\frac{\mu_p G_E^p}{G_M^p}\right)$	0.011

[a] Defined here as the fraction of all coincidence events that passed FPP event selection cuts.

magnetic field uncertainties (largest known source), uncertainties attributable to errors in the polar and azimuthal angle reconstruction in the polarimeter, and uncertainties due to the estimation and subtraction of the residual inelastic background contamination in the final elastic event sample. Other uncertainties include the knowledge of the beam energy, and the "standard", model-independent radiative corrections to the polarization transfer ratio, which tend to be negligible for the cuts used in typical polarization transfer experiments [9]. The detailed breakdown of the major known sources of systematic uncertainty for the Hall C GEp-III/GEp-2γ experiments given in Ref. [45] is instructive in estimating the systematic error budget for this proposal.

TABLE II. Anticipated systematic uncertainty contributions to R_p and their estimated magnitudes. See text for details.

Contribution	Estimated $\Delta_{syst}(R_p)$
Proton kinematic reconstruction	2×10^{-3}
Precession uncertainty due to magnetic field uncertainty	5×10^{-3}
Azimuthal angle reconstruction	10^{-3}
Inelastic background	$< 10^{-3}$
Beam Energy	5×10^{-4}
Radiative Corrections ("standard")	$< 10^{-3}$
Total	6×10^{-3}

Table II lists all major anticipated sources of systematic uncertainty for the proposed measurement, which are estimated based on past experience, taking into account the important differences between the SBS setup and previous Hall A and C measurements that used focusing, small-acceptance spectrometers. At the proposed Q^2 and beam energy, and given the expected detector resolutions, the inelastic background contamination after exhausting all available exclusivity cuts is expected to be essentially negligible, so the estimated contribution of 10^{-3} to the form factor ratio uncertainty should be regarded as a worst-case/upper limit. While the spin precession calculation in SBS is qualitatively simpler than in previous experiments with focusing spectrometers, its ultimate accuracy still depends on the accuracy of the calculated field map used to track proton spins through the GEANT4 setup using the BMT equation. Experience with BigBite and SBS during the neutron form factor experiments shows that the calculated field maps of BigBite and SBS are reliable, given accurate magnet and detector surveys, and accurate knowledge of the location and orientation of the tracking detectors relative to the magnet and the origin of Hall A. The accuracy of the calculated field map can be verified by partially mapping its field in a few key regions/reference points. The tracking detectors can be precisely located and oriented in the Hall using dedicated low-current runs on a thin Carbon foil with the magnet turned off, such that the thin foil acts as a "point source" of straight-line tracks from the

target. Other measurements using the "self-calibrating" $ep \to ep$ reaction allow various redundant and independent cross checks of the spectrometer optics and spin transport calculations. Given the current level of understanding of the SBS and BigBite magnet optics, we very conservatively estimate the systematic uncertainty associated with the knowledge of the magnetic field to be 5×10^{-3} in the final form factor ratio R_p of Eq. (10). Even with the most conservative possible estimate of the systematic uncertainty, the proposed measurement will be statistics-limited, and one may reasonably argue that the proposed measurement, with its high *statistical* precision, serves an important secondary purpose of controlling the systematic errors associated with the three approved higher-Q^2 measurements in E12-07-109. Generally speaking, the sensitivity of the form factor ratio to uncertainties affecting the precession calculation increases at large Q^2.

VI. SUMMARY AND BEAM TIME REQUEST TO PAC52

In summary, we propose adding two PAC days to the 45 PAC days already scheduled for the upcoming SBS GEP run. This small additional beam time would enable an opportunistic, high-precision measurement of $\mu_p G_E^p/G_M^p$ at $Q^2 = 3.7$ GeV^2, needed for comparison to a future positron measurement as described in LOI12-23-008. This measurement would improve the precision of the polarization transfer data at this Q^2 by a factor of 4. It would also significantly enhance the productivity of the GEP run, currently scheduled to begin this fall, by providing an "anchor" Q^2 point of high statistical precision to control systematic uncertainties of the higher-Q^2 measurements.

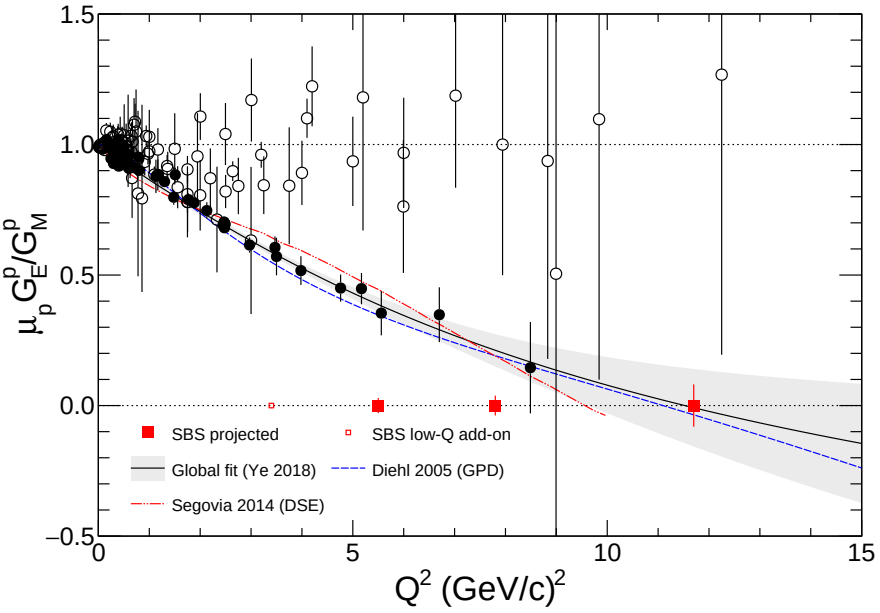

FIG. 11. Projected results of "enhanced" E12-07-109 with the proposed additional Q^2 point, compared to existing data and selected theoretical models. The global fit curve is from Ref. [46]. The two theoretical curves shown are the GPD-based calculation of Ref. [47] and the Dyson-Schwinger Equation calculation of Ref. [48].

TABLE III. Kinematics, projected accuracy and beam time allocations for "GEP+". The projected statistical uncertainties in the form factor ratio include the assumption of 70% overall event reconstruction efficiency due to the combined efficiencies of the individual detectors, including DAQ dead-time.

Status	E_{beam}, GeV	Q^2 range, GeV^2	$\langle Q^2 \rangle$ GeV^2	θ_{ECAL} degrees	$\langle E'_e \rangle$, GeV	θ_{SBS} degrees	$\langle P_p \rangle$ GeV	$\langle \sin\chi \rangle$	Event rate Hz	Days (PAC)	$\Delta(\mu G_E/G_M)$ (statistical)
Proposed	4.3	3.1-4.4	3.7	35.0	2.35	28.5	2.73	0.55	882	2	0.011
Approved/scheduled	6.4	4.5-7.0	5.5	29.8	3.66	25.7	3.77	0.72	291	2	0.029
Approved/scheduled	8.5	6.5-10.0	7.8	27.5	4.64	22.1	5.01	0.84	72	11	0.038
Approved/scheduled	10.6	10.0-14.5	11.7	30.0	4.79	16.9	7.08	0.99	13	32	0.081

.

Figure 11 shows the projected Q^2 points and statistical uncertainties of E12-07-109 with the proposed add-on measurement, compared to existing data and selected theoretical predictions. Table III shows the proposed measurement together with the approved kinematics of E12-07-109 [41, 42]

---

[1] A. J. R. Puckett, J. C. Bernauer, and A. Schmidt, Eur. Phys. J. A **57**, 188 (2021), arXiv:2104.11879 [nucl-ex].
[2] A. Accardi *et al.*, Eur. Phys. J. A **57**, 261 (2021), arXiv:2007.15081 [nucl-ex].
[3] M. K. Jones *et al.*, Phys. Rev. Lett. **84**, 1398 (2000).
[4] O. Gayou *et al.* (Jefferson Lab Hall A), Phys. Rev. Lett. **88**, 092301 (2002), nucl-ex/0111010.
[5] V. Punjabi *et al.*, Phys. Rev. **C71**, 055202 (2005), [Erratum: Phys. Rev.C71,069902(2005)], arXiv:0501018 [nucl-ex].
[6] A. J. R. Puckett *et al.*, Phys. Rev. Lett. **104**, 242301 (2010).
[7] M. Meziane *et al.* (GEp2gamma), Phys. Rev. Lett. **106**, 132501 (2011), arXiv:1012.0339 [nucl-ex].
[8] A. J. R. Puckett *et al.*, Phys. Rev. **C85**, 045203 (2012), arXiv:1102.5737 [nucl-ex].
[9] A. J. R. Puckett *et al.*, Phys. Rev. **C96**, 055203 (2017), arXiv:1707.08587 [nucl-ex].
[10] A. Afanasev, P. G. Blunden, D. Hasell, and B. A. Raue, Prog. Part. Nucl. Phys. **95**, 245 (2017), arXiv:1703.03874 [nucl-ex].
[11] B. S. Henderson *et al.* (OLYMPUS), Phys. Rev. Lett. **118**, 092501 (2017), arXiv:1611.04685 [nucl-ex].
[12] J. C. Bernauer *et al.* (OLYMPUS), Phys. Rev. Lett. **126**, 162501 (2021), arXiv:2008.05349 [nucl-ex].
[13] I. A. Rachek *et al.*, Phys. Rev. Lett. **114**, 062005 (2015), arXiv:1411.7372 [nucl-ex].
[14] D. Adikaram *et al.* (CLAS), Phys. Rev. Lett. **114**, 062003 (2015), arXiv:1411.6908 [nucl-ex].
[15] D. Rimal *et al.* (CLAS), Phys. Rev. **C95**, 065201 (2017).
[16] C. E. Carlson and M. Vanderhaeghen, Ann. Rev. Nucl. Part. Sci. **57**, 171 (2007), arXiv:0701272 [hep-ph].
[17] P. A. Guichon and M. Vanderhaeghen, Phys.Rev.Lett. **91**, 142303 (2003), arXiv:0306007 [hep-ph].
[18] P. Blunden, W. Melnitchouk, and J. Tjon, Phys.Rev.Lett. **91**, 142304 (2003).
[19] L. W. Mo and Y.-S. Tsai, Rev.Mod.Phys. **41**, 205 (1969).
[20] L. C. Maximon and W. C. Parke, Phys. Rev. C **61**, 045502 (2000), arXiv:nucl-th/0002057.
[21] E. A. Kuraev, V. V. Bytev, S. Bakmaev, and E. Tomasi-Gustafsson, Phys. Rev. **C78**, 015205 (2008), arXiv:0710.3699 [hep-ph].
[22] A. Afanasev *et al.*, (2020), arXiv:2012.09970 [nucl-th].
[23] A. Afanasev *et al.*, Eur. Phys. J. A **60**, 91 (2024), arXiv:2306.14578 [hep-ph].
[24] P. G. Blunden, W. Melnitchouk, and J. A. Tjon, Phys. Rev. **C72**, 034612 (2005).
[25] M. Gorchtein, Phys. Lett. **B644**, 322 (2007).
[26] D. Borisyuk and A. Kobushkin, Phys. Rev. C **78**, 025208 (2008), arXiv:0804.4128 [nucl-th].
[27] D. Borisyuk and A. Kobushkin, Phys. Rev. C **92**, 035204 (2015), arXiv:1506.02682 [hep-ph].
[28] P. G. Blunden and W. Melnitchouk, Phys. Rev. **C95**, 065209 (2017), arXiv:1703.06181 [nucl-th].
[29] J. Ahmed, P. G. Blunden, and W. Melnitchouk, Phys. Rev. C **102**, 045205 (2020), arXiv:2006.12543 [nucl-th].
[30] J. Arrington, W. Melnitchouk, and J. Tjon, Phys. Rev. C **76**, 035205 (2007).
[31] Y. Chen, A. Afanasev, S. Brodsky, C. Carlson, and M. Vanderhaeghen, Phys.Rev.Lett. **93**, 122301 (2004), arXiv:0403058 [hep-ph].
[32] A. V. Afanasev, S. J. Brodsky, C. E. Carlson, Y.-C. Chen, and M. Vanderhaeghen, Phys.Rev. **D72**, 013008 (2005), arXiv:0502013 [hep-ph].
[33] D. Borisyuk and A. Kobushkin, Phys. Rev. D **79**, 034001 (2009), arXiv:0811.0266 [hep-ph].
[34] N. Kivel and M. Vanderhaeghen, Phys. Rev. Lett. **103**, 092004 (2009), arXiv:0905.0282 [hep-ph].
[35] N. Kivel and M. Vanderhaeghen, JHEP **04**, 029, arXiv:1212.0683 [hep-ph].
[36] Y.-C. Chen, C.-W. Kao, and S.-N. Yang, Phys. Rev. **B652**, 269 (2007).
[37] D. Borisyuk and A. Kobushkin, Phys. Rev. D **83**, 057501 (2011), arXiv:1012.3746 [hep-ph].
[38] J. Guttmann, N. Kivel, M. Meziane, and M. Vanderhaeghen, Eur. Phys. Jour. **A47**, 1 (2011).
[39] J. Bernauer *et al.* (A1), Phys. Rev. **C90**, 015206 (2014).
[40] A. Schmidt, J. Phys. G **47**, 055109 (2020), arXiv:1907.07318 [nucl-ex].
[41] E. Brash, E. Cisbani, M. Jones, M. Khandaker, L. Pentchev, C. F. Perdrisat, V. Punjabi, B. Wojtsekhowski, *et al.* (2007), `http://www.jlab.org/exp_prog/proposals/07/PR12-07-109.pdf`.
[42] E. Cisbani, M. K. Jones, N. Liyanage, L. P. Pentchev, A. J. R. Puckett, and B. Wojtsekhowski (2019), `https://puckett.physics.uconn.edu/wp-content/uploads/sites/1958/2019/08/gep_update.pdf`.
[43] S. N. Basilev *et al.*, Eur. Phys. J. **A56**, 26 (2020), arXiv:1908.06159 [nucl-ex].
[44] M. E. Christy *et al.*, arXiv (2021), `https://arxiv.org/abs/2103.01842`, arXiv:2103.01842 [nucl-ex].
[45] A. J. R. Puckett *et al.* (GEp-III, GEp-2Gamma), Nucl. Instrum. Meth. A **910**, 54 (2018), arXiv:1707.07750 [nucl-ex].
[46] Z. Ye, J. Arrington, R. J. Hill, and G. Lee, Phys. Lett. **B777**, 8 (2018), arXiv:1707.09063 [nucl-ex].
[47] M. Diehl, T. Feldmann, R. Jakob, and P. Kroll, Eur. Phys. J. **C39**, 1 (2005), arXiv:hep-ph/0408173 [hep-ph].
[48] J. Segovia, I. C. Cloet, C. D. Roberts, and S. M. Schmidt, Few Body Syst. **55**, 1185 (2014), arXiv:1408.2919 [nucl-th].